Physics Letters B 673 (2009) 24–29

Contents lists available at ScienceDirect

Physics Letters B

www.elsevier.com/locate/physletb

BFKL and CCFM evolutions with saturation boundary

Emil Avsar, Edmond Iancu *

Institut de Physique Théorique de Saclay, F-91191 Gif-sur-Yvette, France

ARTICLE INFO

Article history:
Received 6 February 2009
Accepted 8 February 2009
Available online 11 February 2009
Editor: L. Alvarez-Gaumé

ABSTRACT

We perform numerical studies of the BFKL and CCFM equations for the unintegrated gluon distribution supplemented with an absorptive boundary which mimics saturation. For BFKL, this procedure yields the same results for the saturation momentum and the gluon distribution above saturation as the non-linear BK equation, for both fixed and running coupling, and for all the considered energies. This similarity goes beyond expectations based on the correspondence with statistical physics, which hold only for fixed coupling and asymptotically high energies. For the CCFM equation, whose non-linear generalization is not known, our method provides the first study of the approach towards saturation. We find that, in the running-coupling case, the CCFM and BFKL predictions for the energy dependence of the saturation momentum are identical within our numerical accuracy.

1. Introduction

The imminent high-energy experiments at LHC will considerably enlarge the phase-space where the unitarity corrections to QCD interactions, like gluon saturation and multiple scattering, are expected to be important. Such corrections should in particular influence some 'hard' observables, like jet production at forward rapidities, whose theoretical description lies within the realm of perturbative QCD. The jets to be measured at LHC will be relatively 'hard', with virtualities $Q \geqslant 10$ GeV, but because of the high-energy kinematics, their description may go beyond the standard pQCD formalism at high Q^2 — the DGLAP evolution of the parton distributions together with the collinear factorization of the hadronic cross-sections. Rather, the high-energy evolution, of the BFKL [1] or CCFM [2] type, and the associated k_T-factorization scheme should prevail whenever the energy logarithms $\ln s \sim Y$ are larger than the momentum ones, $\ln Q^2$. Besides, this evolution is expected to be amended by non-linear effects reflecting gluon saturation and multiple scattering [3–6]. Such effects can make themselves felt even at relatively large momenta Q, well above the saturation momentum Q_s (the characteristic scale for the onset of unitarity corrections), via phenomena like geometric scaling [9–13]. The saturation scale Q_s grows, roughly, like a power of the energy: $Q_s^2 \sim s^\lambda$ with $\lambda \simeq 0.25$ from fits to HERA data [14]. For forward jet production in proton–proton collisions at LHC, Q_s is expected in the ballpark of 2 to 3 GeV. Besides, much higher values of Q_s can be effectively reached [15] by focusing on 'hot spots' in some rare events, so like Mueller–Navelet jets.

It is therefore important and urgent to provide realistic, quantitative, predictions for the effects of saturation on relatively hard ($Q^2 \gg Q_s^2$) observables at LHC. The restriction to high Q^2 entails some important simplifications, which are essential for the strategy that we shall propose in this Letter.

First, this implies that one can neglect the complex many-body correlations which develop at saturation ($Q \lesssim Q_s$). Hence, the standard k_T-factorization of the hadronic cross-sections still applies, but with modified unintegrated gluon distributions, which reflect saturation. This opens the possibility to include the effects of saturation within Monte Carlo event generators based on k_T-factorization, so like CASCADE [16].

Second, this means that the saturation effects in the gluon distribution and, in particular, the saturation momentum itself can be computed without a detailed knowledge of the non-linear dynamics responsible for unitarization. Rather, they are fully determined by the *linear* evolution if the latter is supplemented with an absorptive boundary condition at low momenta, which plays the role of the saturation momentum and is self-consistently determined by the evolution [10–12]. This property is both important and highly non-trivial. It is important as it allows one to perform studies of saturation even for evolution equations whose non-linear generalizations are not known, so like CCFM evolution, and also BFKL beyond the leading-order approximation. It is furthermore non-trivial, since the high-energy evolution is non-local in transverse momenta, hence the growth in the gluon distribution at high momenta $k_\perp \gg Q_s$ could be feeded by radiation from lower momenta $k_\perp \lesssim Q_s$. This is clearly the case for the linear evolution with running coupling, where the gluon distribution grows faster in the infrared and then acts as a source for gluons with high $k_\perp$.

Yet, at least for a *fixed coupling* and for *asymptotically high energies*, it has been firmly established that the high-energy evolution

* Corresponding author.
E-mail addresses: emil.avsar@cea.fr (E. Avsar), edmond.iancu@cea.fr (E. Iancu).

0370-2693
doi:10.1016/j.physletb.2009.02.011

towards saturation is indeed driven by the linear evolution in the dilute tail of the gluon distribution at $k_\perp \gg Q_s$. The respective argument is based on a correspondence between high-energy QCD and statistical physics [13,17], which however fails to apply in the more realistic case of a *running coupling* [18]. For the latter, our subsequent numerical results will provide the first unambiguous evidence in that sense. Most precisely, we shall find that the BFKL equation with saturation boundary provides exactly the same results for the saturation momentum $Q_s(Y)$ and for the gluon distribution at $k_\perp \geqslant Q_s(Y)$ as the non-linear Balitsky–Kovchegov (BK) equation [3,4], and this for both fixed and running coupling, and for all the considered rapidities $Y \leqslant 120$ — including lower values $Y \leqslant 14$, as relevant for the phenomenology at LHC.

But the BFKL evolution, to be discussed in Section 2, will merely serve as a playground to test our method for numerically implementing the saturation boundary condition within a generic linear evolution. Our main interest is rather in the CCFM evolution, that we shall discuss in Section 3, and which stays at the basis of Monte Carlo event generators [16]. There are at least two reasons why the CCFM evolution is a privileged tool in that respect. First, it takes into account the quantum coherence between successive emissions, and thus allows for a more realistic description of the final state than the BFKL evolution. Second, it provides an interpolation between BFKL dynamics at small x and (approximate) DGLAP dynamics at larger x, which might be essential for most of the "small-x" phase-space to be experimentally accessible at LHC.

By supplementing the CCFM equation with the saturation boundary condition, we shall perform the first study of the CCFM evolution towards saturation, on the example of the unintegrated gluon distribution. To be able to follow the respective evolution up to relatively high rapidities, we shall consider a slightly simplified version of the CCFM equation, that we shall briefly derive (more details will be presented somewhere else [19]). One of our most interesting results is that, in the running coupling case, the CCFM evolution in the presence of saturation provides almost identical results — for the saturation momentum and the gluon distribution at momenta $k_\perp \gtrsim Q_s$ — as the respective BFKL evolution. Our prescription for introducing the saturation boundary condition can be straightforwardly implemented within a Monte Carlo event generator using k_T-factorization [20].

2. BFKL evolution with saturation boundary

In this section we shall explain our method for effectively implementing saturation within a unitarity-violating linear evolution on the example of the BFKL equation [1]. This will allow us to test our method by comparing with the non-linear generalization of the BFKL equation which obeys unitarity — the Balitsky–Kovchegov (BK) equation [3,4]. Although our numerical studies will be performed in (transverse) momentum space, it is more convenient to explain the method in coordinate space. Then, the BK equation describes the high-energy evolution of the scattering amplitude $T(Y,r)$ of a small quark–antiquark dipole with transverse size r. We shall assume the target to be infinite and homogeneous in transverse directions, so we can ignore the impact-parameter dependence of the scattering amplitude and average over angles. The corresponding equation reads

$$\frac{\partial T(Y,r)}{\partial Y} = \frac{\bar\alpha_s}{2\pi}\int \mathrm{d}^2\boldsymbol{z}\,\frac{r^2}{z^2(\boldsymbol{r}-\boldsymbol{z})^2} \times\Big\{-T(Y,r)+T(Y,z)+T\big(Y,|\boldsymbol{r}-\boldsymbol{z}|\big) - T(Y,z)T\big(Y,|\boldsymbol{r}-\boldsymbol{z}|\big)\Big\}. \tag{2.1}$$

Here $\bar\alpha_s \equiv \alpha_s N_c/\pi$, and $\boldsymbol{z}$ and $\boldsymbol{r}-\boldsymbol{z}$ are the transverse sizes of the two dipoles into which the parent dipole $\boldsymbol{r}$ has dissociated before scattering off the target. The last term, quadratic in T, in the r.h.s. of the equation describes multiple scattering and is responsible for unitarization. With this last term omitted, (2.1) reduces to the BFKL equation, which describes the unlimited (exponential) growth of the scattering amplitude with Y and the symmetric expansion of the support of $T(Y,r)$ in r towards both small and large dipole sizes. Note however that the transverse non-locality in Eq. (2.1) is quite weak and can be described as diffusion in the logarithmic variable $\rho \equiv \ln(r_0^2/r^2)$. Here, r_0 is an arbitrary scale of reference.

However, the fully non-linear equation (2.1) preserves (and actually saturates) the unitarity bound $T \leqslant 1$, as $T=1$ is manifestly a fixed point. Because of that, the respective evolution is *asymmetric* in r (or ρ): the solution $T(Y,r)\equiv T(Y,\rho)$ looks like a *front*, which interpolates between $T=1$ at relatively small ρ and $T=0$ at $\rho\to\infty$, and which propagates towards larger values of ρ when increasing Y. Behind the front, the scattering amplitude has reached the 'black disk' limit $T=1$ and thus cannot grow anymore. Ahead of the front, the amplitude is still weak, $T\ll 1$, so the non-linear term in Eq. (2.1) is unimportant. The position $\rho_s(Y)\equiv\ln(r_0^2Q_s^2(Y))$ of the front at 'time' Y, i.e. the value of ρ where T becomes of $\mathcal{O}(1)$, defines the *saturation momentum* $Q_s^2(Y)$ — the scale where unitarity corrections become important at rapidity Y.

Our subsequent results will demonstrate that the progression of the saturation front towards larger values of ρ is driven by the BFKL evolution of the dilute tail at $\rho\gg\rho_s(Y)$ — the front is 'pulled' by its tail. As explained in the Introduction, this property is highly non-trivial, especially at running coupling: the growth of the coupling with decreasing momenta, or increasing dipole sizes, amplifies the contribution of the latter to the evolution, which then becomes asymmetric even in the absence of saturation. In fact, the BFKL evolution with running coupling is infrared-unstable, in the sense that it requires an infrared cutoff to avoid the blow-up of the QCD coupling at $k_\perp\sim\Lambda_{\rm QCD}$, and the final results are strongly sensitive to the value of this cutoff. In view of that, the perturbative framework becomes questionable and, besides, one may expect the associated saturation front — as generated after enforcing unitarity in the BFKL equation with a running coupling — to be of the 'pushed' type.

Yet, as our numerical solutions will explicitly show, this is actually not the case: the saturation front remains of the 'pulled' type even for a running coupling. This is so because the gluon modes with $k_\perp \lesssim Q_s(Y)$ become inert due to saturation, so the evolution is again driven by the dilute tail at high momenta, so like for fixed coupling. In particular, the infrared problem is automatically avoided: the saturation scale effectively acts as an infrared cutoff, which becomes 'hard' ($Q_s^2(Y)\gg\Lambda^2_{\rm QCD}$) for sufficiently high energy. This opens the way towards realistic studies of the front dynamics within the context of the *linear* evolution, as originally suggested in Refs. [10,11]. To that aim, the linear evolution equations must be supplemented with an appropriate *saturation boundary condition*, that we now describe.

Such a boundary condition must ensure that the amplitude never becomes bigger than one. By itself, the position of the front is not *a priori* known, but must be determined when solving the equation. To that aim, let us first introduce a line of constant amplitude $\rho=\rho_c(Y)$ via the condition

$$T\big(Y,\rho=\rho_c(Y)\big)=c, \tag{2.2}$$

where the number c is strictly smaller than one, but not *much* smaller. (The *saturation line* $\rho_s(Y)$ would correspond to $c\sim 1$.) For $\rho<\rho_c(Y)$ and sufficiently high energy, the solution $T_{\rm BFKL}(Y,\rho)$ to the BFKL equation would become larger than one — in fact, arbitrarily large. If this equation is to be solved numerically, one may think about identifying the point $\rho_c(Y)$ numerically at each step in Y, and then enforcing the unitarity limit $T=1$ for any ρ which is smaller than $\rho_c(Y)$ and sufficiently far below it — say, for $\rho\leqslant\rho_c(Y)-\Delta$ with $\Delta\simeq\ln(1/c)$ a number of $\mathcal{O}(1)$. However, this

would not be a very good strategy in practice, since $T = 1$ is not a fixed point for the BFKL equation, so an amplitude of $\mathcal{O}(1)$ would be exponentially amplified by the subsequent evolution. Even if, at small ρ, one cuts off by hand this evolution step-by-step, it is still possible that the spurious radiation from small ρ will affect the tail of the front at large ρ. To avoid that, it is preferable to follow Ref. [11] and enforce the amplitude to *vanish* for $\rho \leqslant \rho_c(Y) - \Delta$:

$$T(Y,\rho) = 0 \quad \text{for } \rho \leqslant \rho_c(Y) - \Delta. \tag{2.3}$$

Since $T = 0$ is a fixed point for the BFKL equation, no further evolution is possible in the 'saturated domain' on the left of $\rho_c(Y) - \Delta$, as it should. When decreasing ρ below $\rho_c(Y)$, the solution $T(Y,\rho)$ will typically start by rising, then reach a maximum $T_{\max} \sim \mathcal{O}(1)$, and eventually decrease to zero. We shall conventionally identify the *saturation scale* $\rho_s(Y)$ with the position of this maximum. In this procedure, the numbers c and Δ are to be viewed as free parameters, which are correlated with each other, since $\Delta \sim \ln(1/c)$.

To describe our numerical results, let us first shift to the momentum representation, and introduce the 'unintegrated gluon distribution' $\mathcal{A}(Y,k)$ — the quantity which enters the calculation of a cross-section via k_T-factorization. For the present purposes, $\mathcal{A}(Y,k)$ can be defined as the following Fourier transform of the dipole amplitude [10]

$$\mathcal{A}(Y,k) = \int \frac{\mathrm{d}^2\boldsymbol{r}}{2\pi r^2} \mathrm{e}^{-i\boldsymbol{k}\cdot\boldsymbol{r}} T(Y,r). \tag{2.4}$$

With this definition, the 'integrated' gluon distribution is obtained as

$$xg\big(x, Q^2\big) = \frac{4N_c^2}{\pi^2\bar{\alpha}_s} \int^{Q^2} \frac{\mathrm{d}^2\boldsymbol{k}}{(2\pi)^2} \int \mathrm{d}^2\boldsymbol{b}\, \mathcal{A}(Y,\boldsymbol{k},\boldsymbol{b}). \tag{2.5}$$

For a homogeneous target, $\mathcal{A}(Y,\boldsymbol{k},\boldsymbol{b}) \equiv \mathcal{A}(Y,k)$, and the above integral over $\boldsymbol{b}$ simply yields the hadron area πR^2. The momentum-space version of the BK equation is particularly simple in that the non-linear term is now local:

$$\frac{\partial}{\partial Y}\mathcal{A}(Y,k) = \bar{\alpha}_s \int \frac{\mathrm{d}^2\boldsymbol{q}}{\pi} \frac{1}{q^2(\boldsymbol{k}-\boldsymbol{q})^2} \left(q^2\mathcal{A}(Y,q) - \frac{k^2}{2}\mathcal{A}(Y,k)\right) - \bar{\alpha}_s\big(\mathcal{A}(Y,k)\big)^2. \tag{2.6}$$

In what follows, we shall compare the numerical solutions to this equation, with both fixed and running coupling, to the corresponding solutions for the BFKL equation supplemented with the boundary condition[1] in Eqs. (2.2), (2.3).

For the fixed coupling calculations we shall use $\bar{\alpha}_s = 0.2$. To include running coupling effects, we shall pull the $\bar{\alpha}_s$ factor inside the q-integral in Eq. (2.6) and use the one-loop expression for the running coupling with scale $Q^2 = \max(k^2, q^2)$ and $\Lambda_{\mathrm{QCD}} = 200$ MeV. This simple prescription is in agreement with the recently constructed running-coupling version of the BK equation [7,8]. To avoid the infrared divergence of the coupling at $Q^2 = \Lambda^2_{\mathrm{QCD}}$, we shall replace $\alpha_s(Q^2) \to \alpha_s(Q^2 + \mu^2)$ for some parameter μ. Our default choice will be $\mu^2 = 0.5$ GeV^2, but we shall study the sensitivity of our results to variations in μ. Our initial condition reads $\mathcal{A}(Y = 0, k) = 1/2k^2$ (bremsstrahlung) for $k > 1$ GeV and $\mathcal{A}(Y = 0, k) = 0$ for $k < 1$ GeV.

For the fixed coupling case, our results are displayed in Fig. 1 for six values of the rapidity within the range $20 \leqslant Y \leqslant 70$ and for two different choices for the parameters c and Δ. The most important observation about these results is that the saturation fronts generated by the two types of evolution do precisely coincide with each other for all momenta $\rho \geqslant \rho_c(Y) - \Delta$, and for all the considered rapidities. This property is not altered by changing the values for c and (correlated to it) for Δ. We have also checked that our numerical results are consistent with the analytic estimate of the saturation momentum at fixed coupling; namely, for sufficiently large Y one expects $\rho_s \simeq \lambda_f \bar{\alpha}_s Y$ with $\lambda_f \approx 4.88$ [10,11], and this is indeed verified by our curves in Fig. 1.

We now turn to the more realistic case of a running coupling. Then, as alluded to before, the pure BFKL evolution is infrared unstable, and indeed we see a marked difference between the results of the linear evolution and those of the non-linear one, even at very high k. This is exhibited in Fig. 2 where we compare the strict BFKL evolution to the BK one, and also to the BFKL evolution with the absorptive boundary. Once again, there is a perfect matching between the saturation fronts provided by BK and, respectively, BFKL with saturation boundary. From these curves, it is also possible to extract the Y-dependence of the saturation momentum $\rho_s(Y)$ for running coupling. We find that the squared-root law $\rho_s \simeq \lambda_r\sqrt{Y}$ predicted by the theory [10–12] for asymptotically large Y provides a good fit to our numerical results, with a fitted value $\lambda_r \simeq 2.9$ which agrees reasonably well with the respective theoretical expectation $\lambda_r \simeq 3.2$.

Now, from the phenomenological point of view, we are more interested in values of Y which are not that large, say $Y \leqslant 14$ (corresponding to $x \gtrsim 10^{-6}$), as relevant for forward jet production at LHC. With that in mind, we also show in Fig. 2 (right) the results for lower values of Y, between 6 and 14 units; one can thus see that the absorptive boundary method works equally well also for such lower rapidities.

We have furthermore tested the sensitivity of our results to the value of the IR cutoff μ^2 inserted in the running coupling. Unlike the pure BFKL results, which are extremely sensitive to a change in μ, the results obtained after enforcing the saturation boundary show no sensitivity whatsoever [19].

3. CCFM evolution with saturation boundary

In this section we shall present a compact version of the CCFM equation [2] to which we shall apply the boundary condition described in the previous section. A more comprehensive discussion of the CCFM formalism and its relation to BFKL will be given elsewhere [19], together with more detailed numerical studies, of which the present Letter is only giving a glimpse.

The CCFM evolution takes into account the quantum coherence between successive emissions via angular ordering in the parton cascades. Accordingly, the respective gluon distribution now depends upon three variables, $\mathcal{A} = \mathcal{A}(x,k,\bar{q})$, where the third variable $\bar{q}$ is a transverse momentum related to the maximum angle which determines the phase space where emissions are allowed. This angle is set by the hard scattering of the space-like photon against a quark inside the proton. It is customary to define the variable ξ which is the squared angle, $\xi \equiv q^2/(y^2E^2)$, where q is the transverse momentum of a gluon emitted in the s-channel, y is its longitudinal momentum fraction, and E is the energy of the proton; then, all emissions must satisfy $\xi \leqslant \bar{\xi} \equiv \bar{q}^2/(x^2E^2)$.

The CCFM equation for $\mathcal{A}$ can be written in different versions, depending on how 'exclusive' we choose the gluon distribution to be. That is, so long as one is not interested in the structure of the final state, one can 'integrate out' some of the emissions in the s-channel, as they do not change the overall (unintegrated) gluon distribution (and hence neither the probability for the interaction with a projectile). In practice, this amounts to suitable cancellations between 'real' gluon emissions and 'virtual' (or 'Sudakov') terms.

[1] The boundary condition for $\mathcal{A}(Y,k)$ is similar to that for $T(Y,r)$ in Eqs. (2.2), (2.3) because, with the normalization in Eq. (2.4), the saturation effects in the gluon distribution become important when $\mathcal{A}(Y,k) \sim \mathcal{O}(1)$.

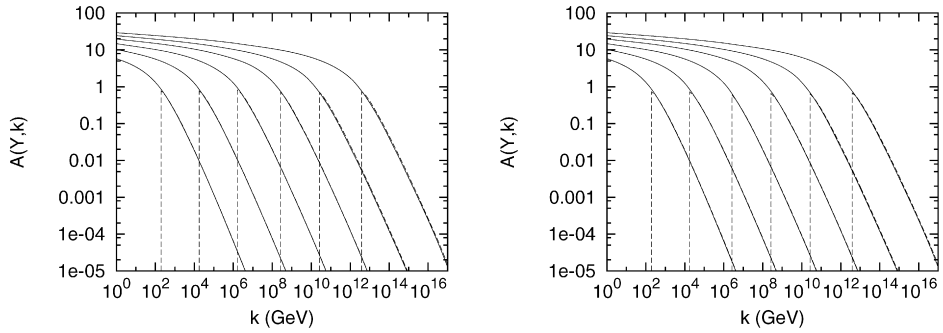

Fig. 1. The solutions of the BK equation (2.6) (solid lines) vs. those of the BFKL equation with absorptive boundary condition (dashed lines), for $Y = 20$, 30, 40, 50, 60, and 70. We have chosen $c = 0.1$ and $\Delta = 5.0$ for the figure on the left and, respectively, $c = 0.3$ and $\Delta = 3.0$ for that on the right.

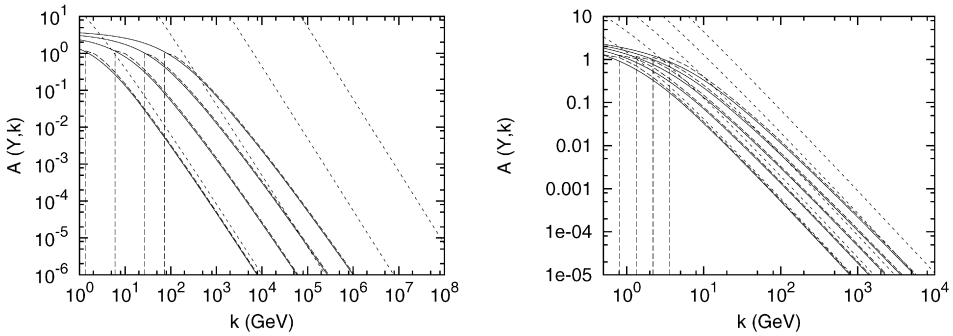

Fig. 2. The running coupling results for: BK (solid curves), BFKL with absorptive boundary (long dashed curves) and pure BFKL (short dashed curves) for (left) $Y = 10, 20, 30$ and 40, and (right) $Y = 6, 8, 10, 12$ and 14. For the absorptive boundary we used $c = 0.1$ and $\Delta = 5.0$.

If one keeps within $\mathcal{A}$ only the emissions associated with the $1/z$ pole in the splitting function, then the CCFM equation can be written as the following integral equation

$$\mathcal{A}(x,k,\bar{q}) = \bar{\alpha}_s \int_x^1 \frac{\mathrm{d}z}{z} \int \frac{\mathrm{d}^2\boldsymbol{q}}{\pi q^2}\theta(\bar{q}-zq)\Delta_{ns}(k,z,q) \times \mathcal{A}\left(\frac{x}{z},|\boldsymbol{k}+\boldsymbol{q}|,p\right), \tag{3.7}$$

where $\boldsymbol{q}$ and $1-z$ are, respectively, the transverse momentum and the energy fraction of the 'real' gluon emitted (in one step of the evolution) in the s-channel.[2] The theta function comes from the angular ordering constraint $\xi \leqslant \bar{\xi}$. There is also an energy ordering implicit in (3.7): emissions are ordered in energy as well as in angle. Finally, Δ_{ns} is the so-called 'non-Sudakov form factor', which accounts for virtual corrections and is necessary to ensure probability conservation

$$\Delta_{ns}(z,k,q) = \exp\left(-\bar{\alpha}_s \int_z^1 \frac{\mathrm{d}z'}{z'} \int_{z'^2q^2}^{k^2} \frac{\mathrm{d}q'^2}{q'^2}\right) = \exp\left(-\bar{\alpha}_s \log\frac{1}{z}\log\frac{k^2}{zq^2}\right). \tag{3.8}$$

Since $\mathcal{A}$ now depends upon three variables, Eq. (3.7) is much more difficult to solve than the BFKL equation. To simplify the numerics and thus be able to explore a relatively wide range in k and Y, it is convenient to use a simpler version of the CCFM equation, which is obtained — modulo some approximations — by using the non-Sudakov factor to cancel a certain class of real emissions in (3.8) (see also Refs. [21,22]).

Specifically, with reference to the elementary splitting $\boldsymbol{k}' \to \boldsymbol{k} + \boldsymbol{q}$, we have three possibilities: either $k' \approx k \gg q$, or $k' \approx q \gg k$, or, finally, $k \approx q \gg k'$. The emissions satisfying the first condition are the ones which can be canceled against Δ_{ns}. To that aim, we must also include, within the integrand of Eq. (3.7), the so-called *kinematical constraint* $k^2 > zq^2$ which ensures that the squared four-momenta of the virtual propagators are dominated by their transverse part as required by the multi-Regge kinematics. This constraint is generally kept implicit in the CCFM (or BFKL) literature, since the Regge kinematics is guaranteed *to the order of interest*; yet, its explicit inclusion in the equations introduces corrections which are formally of higher order in α_s, but which can be numerically important. After including this constraint, we can remove the factor Δ_{ns} from Eq. (3.7) and simultaneously limit ourselves to emissions satisfying the last two constraints written above, which can be summarized as $\theta(q^2 - \min(k^2, k'^2))$. We thus obtain

$$\mathcal{A}(x,k,\bar{q}) = \bar{\alpha}_s \int_x^1 \frac{\mathrm{d}z}{z} \int \frac{\mathrm{d}^2\boldsymbol{q}}{\pi q^2}\theta(\bar{q}-zq)\theta\big(k^2-zq^2\big) \times \theta\big(q^2-\min\big(k^2,k'^2\big)\big)\mathcal{A}\left(\frac{x}{z},k',q\right). \tag{3.9}$$

Since in practice $\bar{q} \geqslant k$, we further have $\bar{q}^2 \geqslant k^2 \geqslant zq^2 \geqslant z^2q^2$. Therefore the angular ordering is automatic and $\theta(\bar{q}-zq)$ can be neglected. This means that the dependence on the third variable $\bar{q}$ drops out, and we can write

$$\mathcal{A}(x,k) = \bar{\alpha}_s \int_x^1 \frac{\mathrm{d}z}{z} \int \frac{\mathrm{d}^2q}{\pi q^2}\theta\big(k^2-zq^2\big) \times \theta\big(q^2-\min\big(k^2,k'^2\big)\big)\mathcal{A}\left(\frac{x}{z},k'\right). \tag{3.10}$$

[2] Strictly speaking, Eq. (3.7) should involve the rescaled variables $\bar{p} = \bar{q}/(1-x)$ and $\boldsymbol{p} \equiv \boldsymbol{q}/(1-z)$, but here we are only interested in the small-x behaviour, so we make no distinction between e.g. p and q [19].

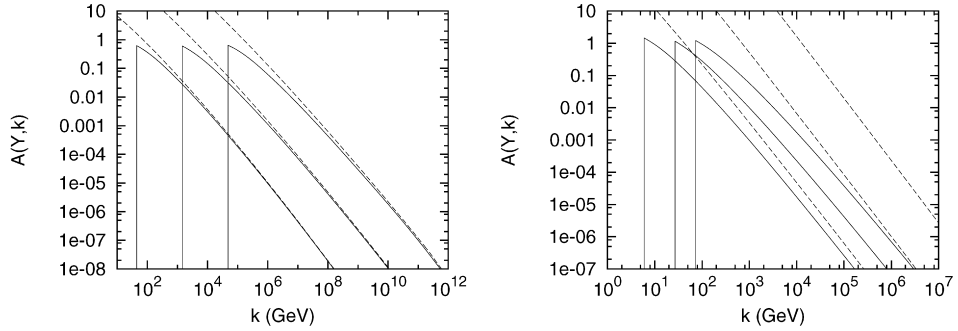

Fig. 3. Comparison between the solutions to the CCFM equation (3.13) with saturation boundary (solid lines) and without it (dashed lines), for $Y = 20, 30$, and 40. Left: fixed coupling $\bar{\alpha}_s = 0.2$. Right: running coupling.

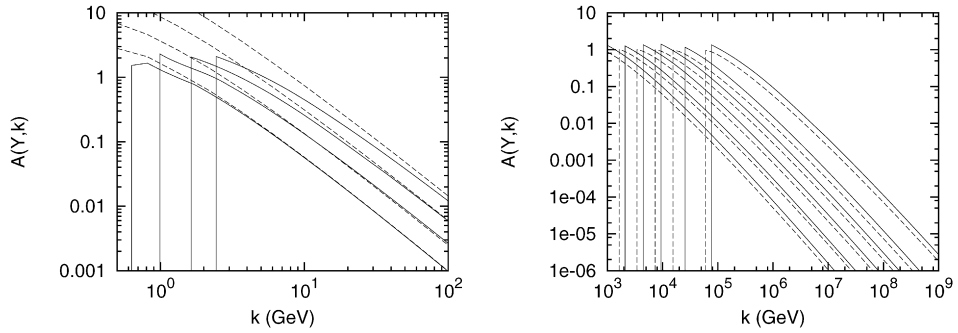

Fig. 4. Left: Solutions to the running-coupling CCFM equation (3.13) with the saturation boundary (solid lines) and without it (dashed lines) for $Y = 8, 10, 12$, and 14. Right: CCFM (solid lines) vs. BFKL (dashed lines) solutions with running coupling and saturation boundary for very high rapidities: $Y = 60, 70, 80, 90, 100$, and 120.

We shall now perform the integration over the azimuthal angle ϕ between $\boldsymbol{q}$ and $\boldsymbol{k}$. After some simple manipulations, one obtains [19]

$$\mathcal{A}(x,k) = \bar{\alpha}_s \int_x^1 \frac{\mathrm{d}z}{z} \int \frac{\mathrm{d}k'^2}{|k'^2 - k^2|} \theta\big(z - xk'^2/k^2\big) h(\kappa) \mathcal{A}(z,k'), \tag{3.11}$$

where $\kappa \equiv \min(k^2, k'^2)/\max(k^2, k'^2)$ and

$$h(\kappa) \equiv 1 - \frac{2}{\pi} \arctan\left(\frac{1+\sqrt{\kappa}}{1-\sqrt{\kappa}} \sqrt{\frac{2\sqrt{\kappa}-1}{2\sqrt{\kappa}+1}}\right) \theta(\kappa - 1/4). \tag{3.12}$$

Notice that $h(\kappa) \to 0$ as $\kappa \to 1$, so Eq. (3.11) has no singularity at $k' = k$. To obtain an integro-differential equation, we define $z = e^{-y}$ and $x = e^{-Y}$ and differentiate the l.h.s. with respect to Y. We thus get

$$\begin{aligned} &\partial_Y \mathcal{A}(Y,k) \\ &\quad = \bar{\alpha}_s \int \frac{\mathrm{d}k'^2}{|k^2 - k'^2|} h(\kappa) \Big(\theta\big(k^2 - k'^2\big) \mathcal{A}(Y,k') \\ &\qquad + \theta\big(k'^2 - k^2\big) \theta\big(Y - \log\big(k'^2/k^2\big)\big) \mathcal{A}\big(Y - \log\big(k'^2/k^2\big), k'\big) \Big), \end{aligned} \tag{3.13}$$

which is our final version for the CCFM equation and is in fact the same as an equation originally proposed in Ref. [21].

It is first interesting to compare the predictions of Eq. (3.13) to those of the BFKL equation for the strictly linear evolution. This will be shown in Ref. [19]. but the main conclusion is that the BFKL evolution is considerably faster. This difference is to be attributed to the non-local term in the r.h.s. of Eq. (3.13): the 'retarded' distribution $\mathcal{A}(Y - \log(k'^2/k^2), k')$ is generally smaller than the 'instantaneous' one $\mathcal{A}(Y, k')$. But even though the CCFM evolution is somewhat slower, Eq. (3.13) still predicts a rapid growth with Y, which in the absence of any non-linearity would lead to unitarity violation. To cure for that, we shall enforce the absorptive boundary condition (2.3) on Eq. (3.13). The corresponding results are compared to those of the purely (CCFM) linear evolution in Fig. 3, for both fixed and running coupling. As in the BFKL case (compare to Fig. 2), the difference is more pronounced for a running coupling, since then the linear evolution is again infrared-unstable, and this instability is removed by the inclusion of saturation.

For the more realistic, running-coupling, case it is furthermore interesting to show the results at lower rapidities, as relevant for LHC. This is exhibited in the leftmost figure in Fig. 4, together with the corresponding results of the strictly linear evolution. As one can see there, for $Y = 14$ and k as high as 10 GeV (which is well above the respective saturation momentum $Q_s \simeq 2.5$ GeV), saturation reduces the predicted gluon distribution by about a factor of 2.

Finally, in the rightmost figure in Fig. 4, we compare the saturation fronts provided by the BFKL and CCFM evolutions with running coupling and for relatively high rapidities, up to $Y = 120$. Remarkably, the BFKL and CCFM results appear to very close to each other, meaning that the corresponding fronts propagate at roughly the same speed. This is at variance with the situation at *fixed* coupling, where the BFKL evolution is still faster.

From our results, we have also extracted the saturation momentum $\rho_s(Y)$ as predicted by the CCFM evolution. We thus found the same types of energy dependence as for BFKL. Trying simple fits of the form $\rho_s = \lambda_f \bar{\alpha}_s Y$ for fixed coupling and, respectively, $\rho_s = \lambda_r \sqrt{Y}$ for running coupling, we find[3] $\lambda_f \approx 3.5$ and $\lambda_r \approx 2.9$. For fixed coupling, this value λ_f is indeed smaller (although not *much* smaller) than the corresponding BFKL estimate $\lambda_f \simeq 4.9$. But

[3] Note that, at fixed coupling, the CCFM estimate for the parameter λ_f defined as above is still a function of $\bar{\alpha}_s$ (unlike the respective BFKL estimate); hence this value $\lambda_f \approx 3.5$ must be seen as the value corresponding to $\bar{\alpha}_s = 0.2$. We shall further discuss the $\bar{\alpha}_s$-dependence of the CCFM parameter λ_f in Ref. [19].

for running coupling, the CCFM and BFKL estimates for λ_r are essentially the same within our numerical accuracy.

It would be of course interesting to understand this similarity between the BFKL and CCFM evolutions towards saturation in more depth, and also to perform more detailed studies of the CCFM evolution with saturation boundary, in order e.g. to explicitly test geometric scaling. We postpone such studies to a further work [19].

Acknowledgements

We would like to thank Al Mueller and Dionysis Triantafyllopoulos for valuable comments on the manuscript. This work is supported in part by Agence Nationale de la Recherche via the programme ANR-06-BLAN-0285-01.

References

[1] L.N. Lipatov, Sov. J. Nucl. Phys. 23 (1976) 338;
E.A. Kuraev, L.N. Lipatov, V.S. Fadin, Zh. Eksp. Teor. Fiz. 72 (1977) 3, Sov. Phys. JETP 45 (1977) 199;
Ya.Ya. Balitsky, L.N. Lipatov, Sov. J. Nucl. Phys. 28 (1978) 822.
[2] M. Ciafaloni, Nucl. Phys. B 296 (1988) 49;
S. Catani, F. Fiorani, G. Marchesini, Phys. Lett. B 234 (1990) 339;
S. Catani, F. Fiorani, G. Marchesini, Nucl. Phys. B 336 (1990) 18.
[3] I. Balitsky, Nucl. Phys. B 463 (1996) 99.
[4] Y.V. Kovchegov, Phys. Rev. D 60 (1999) 034008.
[5] J. Jalilian-Marian, A. Kovner, A. Leonidov, H. Weigert, Nucl. Phys. B 504 (1997) 415;
J. Jalilian-Marian, A. Kovner, A. Leonidov, H. Weigert, Phys. Rev. D 59 (1999) 014014;
J. Jalilian-Marian, A. Kovner, H. Weigert, Phys. Rev. D 59 (1999) 014015;
A. Kovner, J.G. Milhano, H. Weigert, Phys. Rev. D 62 (2000) 114005.
[6] E. Iancu, A. Leonidov, L. McLerran, Nucl. Phys. A 692 (2001) 583;
E. Iancu, A. Leonidov, L. McLerran, Phys. Lett. B 510 (2001) 133;
E. Ferreiro, E. Iancu, A. Leonidov, L. McLerran, Nucl. Phys. A 703 (2002) 489;
E. Iancu, L. McLerran, Phys. Lett. B 510 (2001) 145.
[7] I. Balitsky, Phys. Rev. D 75 (2007) 014001.
[8] Y.V. Kovchegov, H. Weigert, Nucl. Phys. A 784 (2007) 188.
[9] A.M. Stasto, K. Golec-Biernat, J. Kwiecinski, Phys. Rev. Lett. 86 (2001) 596.
[10] E. Iancu, K. Itakura, L. McLerran, Nucl. Phys. A 708 (2002) 327.
[11] A.H. Mueller, D.N. Triantafyllopoulos, Nucl. Phys. B 640 (2002) 331.
[12] D.N. Triantafyllopoulos, Nucl. Phys. B 648 (2003) 293.
[13] S. Munier, R. Peschanski, Phys. Rev. Lett. 91 (2003) 232001.
[14] G. Soyez, Phys. Lett. B 655 (2007) 32.
[15] E. Iancu, M.S. Kugeratski, D.N. Triantafyllopoulos, Nucl. Phys. A 808 (2008) 95.
[16] H. Jung, G.P. Salam, Eur. Phys. J. C 19 (2001) 351.
[17] E. Iancu, A.H. Mueller, S. Munier, Phys. Lett. B 606 (2005) 342.
[18] A. Dumitru, E. Iancu, L. Portugal, G. Soyez, D.N. Triantafyllopoulos, JHEP 0708 (2007) 062.
[19] E. Avsar, E. Iancu, in preparation.
[20] E. Avsar, E. Iancu, K. Kutak, H. Jung, in preparation.
[21] B. Andersson, G. Gustafson, J. Samuelsson, Nucl. Phys. B 467 (1996) 443.
[22] G.P. Salam, JHEP 9903 (1999) 009.